Supporting information

Solid-state in situ constructing Cu_2O/CuO heterostructures with adjustable phase compositions toward promoted CO oxidation activity

Baolin Liu[a], Yizhao Li[a,b*], Kun Wang[a], Yali Cao[a,*]

[a]*Key Laboratory of Energy Materials Chemistry, Ministry of Education, Key Laboratory of Advanced Functional Materials, Autonomous Region, Institute of Applied Chemistry, College of Chemistry, Xinjiang University, Urumqi 830046, Xinjiang, China.*

[b]*College of Chemical Engineering, Xinjiang University, Urumqi 830046, Xinjiang, China.*

[*]*Corresponding author. Tel: +86-991-8583083; Fax: +86-991-8588883;*

E-mails: liyizhao0809@126.com (Y. Li); caoyali523@163.com (Y. Cao).

1. The characterization of catalyst

The structure information of samples was acquired by X-ray powder diffraction (XRD) on Bruker D8 employing Cu-Kα radiation (1.54056 Å) equipped an operating voltage of 40 kV and a beam current of 40 mA. The morphologies of samples were observed by high resolution transmission electron microscope (HRTEM), which was obtained from a JEM-2010F electron microscope with an accelerating voltage of 200 kV. The surface components and structure of samples were characterized by X-ray photoelectron spectra (XPS) (Thermo Fisher Scientific ESCALAB250Xi) employing Al Kα (1486.6 eV). Fourier transform infrared (FT-IR) spectra were obtained on a Bruker EQUINOX55 spectrophotometer in the wave interval between 4000 and 400 cm^{-1}.

The reducibility of catalysts was investigated by H_2 temperature-programmed reduction (H_2-TPR) (XQ 5870 series) measured in a quartz reactor. Typically, 50 mg of samples was pretreated in N_2 stream at 200°C for 30 min before testing, and then they were cooled to room temperature. The gas feed was switched to H_2-N_2 stream where volume fraction of H_2 is 10%. The amount of H_2 consumption and the TPR profile was monitored by a thermal conductivity (TCD) detector and recorded with temperature programming at a rate of 10 °C min^{-1} from room teperature to 500°C. The H_2 consumptions of the reduction band were calibrated by a standard CuO (99.998%) powder.

For O_2 temperature-programmed desorption (O_2-TPD), about 100 mg of catalyst was pretreated in a He stream at 120°C for 1h with a flow rate of 30 mL/min. The temperature was reduced to 30°C and subsequently saturated with 10% O_2 (balanced with He) for 1h, then purged by pure He stream for 1h. Finally, the temperature was heated to 600°C at a rate of 10 °C min^{-1}.

For CO temperature-programmed desorption (CO-TPD), about 100 mg of catalyst was pretreated in a He stream at 120°C for 1h with a flow rate of 30 mL/min. The temperature was reduced to 30°C and subsequently saturated with 10% CO (balanced with He) for 1h, then purged by pure He stream for 1h. Finally, the temperature was heated to 600°C at a rate of 10 °C min^{-1}.

2. The test of catalytic performance

The activity and stability of catalysts toward to CO oxidation was evaluated in a fixed bed quartz reactor at atmospheric pressure. Typically, 100 mg of catalyst without any pretreatment was loaded. The mixed feed gas contained with 1 vol% CO and 20 vol% O_2 in N_2 balance at 50 ml min^{-1} of flow rate (space velocity = 30000 ml $gcat^{-1}$ h^{-1}) was applied to the reactor. The change of gas concentration was monitored with an online gas chromatography system (Agilent 7890B) equipped with a TCD detector. The CO conversion was calculated based on the following formula.

$$CO\ conversion\ (\%) = \frac{[CO]_{in} - [CO]_{out}}{[CO]_{in}} \times 100\%, \quad (1)$$

The reaction rate (R_{CO} (mol g^{-1} s^{-1}) for CO oxidation at certain temperature were calculated by the following the equation:

$$R_{CO} = \frac{X_{CO} V_{CO}}{m}, \quad (2)$$

where X_{CO} is the CO conversion, V_{CO} the CO gas flow rate (in units of mol s^{-1}), and m is the mass of catalyst (in grams).

The apparent activation energies (E_a) are calculated by the Arrhenius Equation: $\ln k = -E_a/RT + \ln A$, when CO conversion lower than 15%, where k stands for the reaction rate constant, R=8.314 J·mol^{-1}·K^{-1}, T for the reaction temperature, A for the Arrhenius factor.

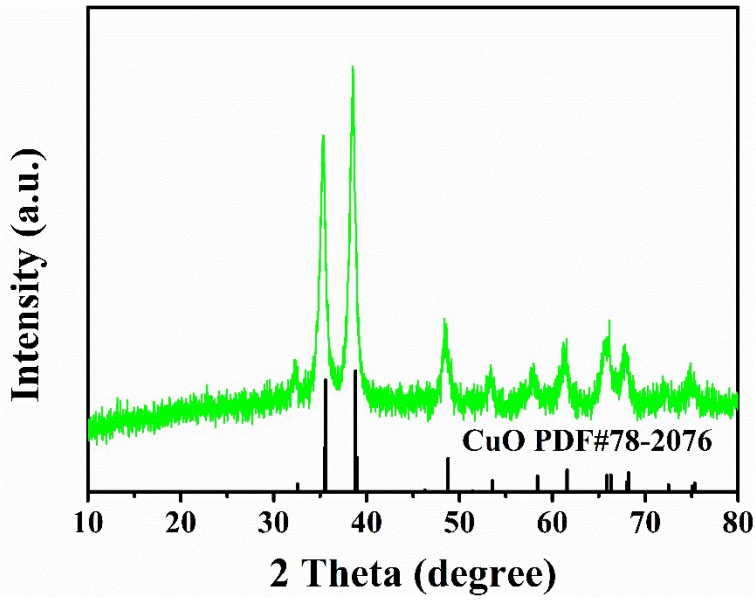

Fig. S1. The powder XRD pattern of CuO catalysts.

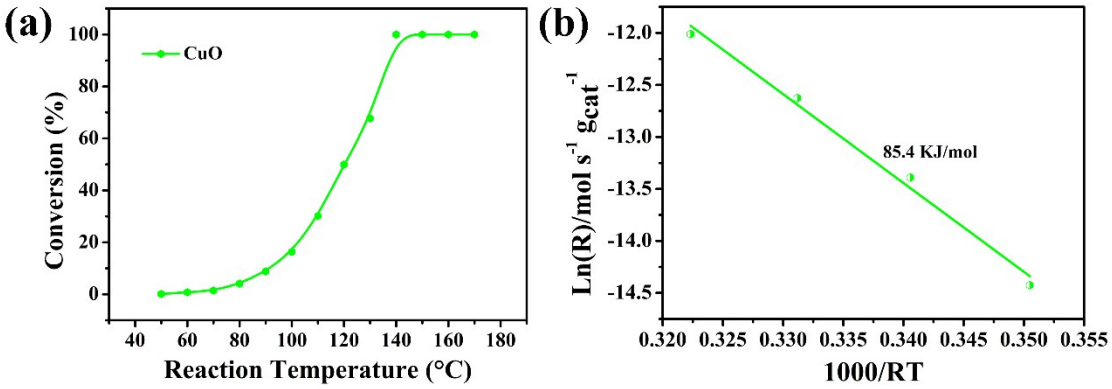

Fig. S2. (a) Light-off curve of CO oxidation; (b) Arrhenius plot and apparent activation energy of CuO catalyst.

Table S1 Quantified differential CO conversion rates of the catalysts at 120°C.

Sample	R at 120°C (mol s^{-1} g^{-1}) ($\times 10^{-5}$)[a]
Cu_2O/CuO-0.5	3.27
Cu_2O/CuO-1	7.39
Cu_2O/CuO-5	30.17
Cu_2O/CuO-7	17.16

[a]R: CO conversion rates normalized by catalyst weights.

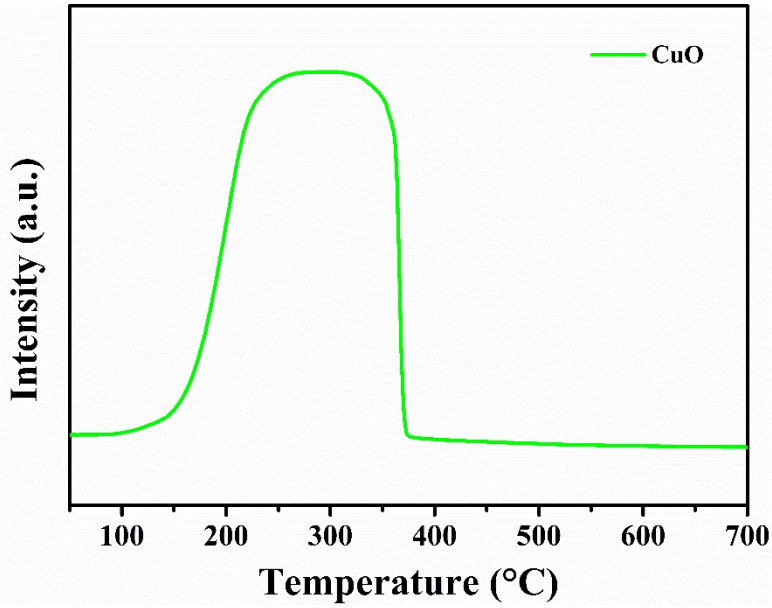

Fig. S3. H_2-TPR result of CuO sample.

Table S2 Catalytic activity of CO oxidation with Cu_2O/CuO heterostructures obtained from different preparation method reported in previous literature.

Sample	method	Amount of catalyst (mg)	Feed gas composition	Flow rate ($mL \cdot min^{-1}$)	T_{50} (°C)	T_{100} (°C)	Ref.
CuO/RGO	Hydrothermal method	400	$CO/O_2/N_2$=10/21/83	73.2	130	165	[1]
CuO nanowires	Heating Cu grids in air	36	$CO/O_2/N_2$=1/16/83	100	300	360	[2]
CuO nanoparticles	precipitation method	50	CO/O_2/He = 4/20/76	60	100	125	[3]
Cu_2O	Solution-phase methods	30+30(SiO_2)	$CO/O_2/N_2$=1/20/79	30	-	240	[4]
Cubic Au-CuO/Cu_2O	chemical precipitation method	200	$CO/O_2/H_2/N_2$ = 1.2/0.8/50/48	50	150	200	[5]
CuO/Cu_2O composites	Solution method	60	CO/O_2/He = 1/6/93	135	175	225	[6]
CuO nanopowders	Precipitation	-	CO/O_2/Ne/He=0.2/1/0.2/98.6	1000	108	150	[7]
Cu-Cu_2O Heterogeneous	Solution method	100	$CO/O_2/N_2$= 1/10/89	100	178	228	[8]
CuO/Cu_2O composites	Hydrothermal method	50	CO/O_2/He = 1/20/79	30	110	140	[9]
Cu_2O-CuO nanospheres	Solution method	100	$CO/O_2/N_2$= 1/3/96	40	117	140	[10]
Cu_2O/CuO heterostructures	Solid-state chemical method	100	$CO/O_2/N_2$ = 1/20/79	50	108	130	This work

References

1. Y. Wang, Z. H. Wen, H. L. Zhang, G. H. Cao, Q. Sun and J. L. Cao, *Catalysts*, 2016, **6**, 1-8.
2. H. Yan, X. Liu, R. Xu, P. lv and P. Zhao, *Mater. Res. Bull.*, 2013, **48**, 2102-2105.
3. A. F. Zedan, A. T. Mohamed, M. S. El-Shall, S. Y. AlQaradawi and A. S. AlJaber, *RSC Advances*, 2018, **8**, 19499-19511.
4. H. Bao, W. Zhang, Q. Hua, Z. Jiang, J. Yang and W. Huang, *Angew. Chem. Int. Ed. Engl.*, 2011, **50**, 12294-12298.
5. C. X. Qi, Y. H. Zheng, H. Lin, H. J. Su, X. Sun and L. B. Sun, *Appl. Catal. B Environ.*, 2019, **253**, 160-169.
6. S. Zhang, H. Liu, C. Sun, P. Liu, L. Li, Z. Yang, X. Feng, F. Huo and X. Lu, *J. Mater. Chem. A*, 2015, **3**, 5294-5298.
7. D. A. Svintsitskiy, T. Y. Kardash, O. A. Stonkus, E. M. Slavinskaya, A. I. Stadnichenko, S. V. Koscheev, A. P. Chupakhin and A. I. Boronin, *J. Phys. Chem. C*, 2013, **117**, 14588-14599.
8. B. Ma, C. C. Kong, J. Lv, X. J. Zhang, S. Yang, T. Yang and Z. M. Yang, *Adv. Mater. Interfaces*, 2020, **7**, 1901643.
9. Y. Yang, H. Dong, Y. Wang, Y. Wang, N. Liu, D. Wang and X. Zhang, *Inorg. Chem. Commun.*, 2017, **86**, 74-77.
10. B. Wei, N. Yang, F. Pang and J. Ge, *The Journal of Physical Chemistry C*, 2018, **122**, 19524-19531.